Transactions of the TSME (2018) Vol. 6, No. 1, 40-49
Journal of Research and Applications in Mechanical Engineering

ISSN 2229-2152 print
DOI: 10.14456/jrame.2018.5

Research Article

INVESTIGATION ON PROFILE OF SLOTS MACHINED BY ELECTROCHEMICAL MILLING WITH HOLLOW ELECTRODE

J. Pattavanitch*
Department of Mechanical Engineering, Faculty of Engineering, Burapha University
169 Long-Hard Bangsaen Rd., Muang, Chonburi, 20131
Thailand

ABSTRACT:
This study investigated the fabrication of slots by electrochemical milling using hollow electrodes. The influence on process performance of different applied voltages, tool feed rates, and tool diameters were studied using experimental and numerical methods. Experimental results showed that a part-sinusoidal profile appeared at the center of the slots bottom face and that machining accuracy depends not only on machining parameters but also on tool diameter. An in-house boundary element program for electrochemical milling process has been developed to predict the shape of slots machined by hollow electrodes in a three-dimensional domain, and the predicted shapes were compared with the actual machined slots, showing agreement between the predicted and experimental results.

Keywords: *Electrochemical machining, Slot milling, BEM, Modelling*

1. INTRODUCTION

Electrochemical machining (ECM) is an unconventional manufacturing technique through which the atoms of an electrically conductive material are removed by means of electrolysis rather than by the thermal effect or by mechanical contact. The main advantages of the ECM process are that the rate of metal removal is independent from the metal hardness and other mechanical properties; there is no tool wear; and there are no residual stresses in the workpiece. This machining technology is used to manufacture parts in many industries, including aerospace [1], automotive [2], medical components [3], and microelectronics [4].

ECM is widely used in cavity die-sinking processes where the pre-shaped tool (cathode) is fed toward the workpiece to generate three-dimensional (3D) shapes. Since the effect of stray current results in more material being removed, the tool has to be slightly different than the shape required on the workpiece. Thus, especially in EC sinking, a considerable amount of effort is required to design the tool, causing the cost of machining to increase.

The difficulties of designing the tool in EC sinking can be eliminated by using EC milling, in which a tool with a simple rectangular, spherical, or cylindrical shape is moved along a specific path to generate the required final shape on the workpiece.

Since ECM is a non-contact type of machining, it is important to be able both to control the process and to predict the diameter of the final workpiece based on process parameters.

* Corresponding author: J. Pattavanitch
E-mail address: jitti@eng.buu.ac.th

Typically in EC milling, a constant or pulse voltage is applied between electrodes. Several researchers have tried to take into account the effect of machining process parameters such as applied voltage and frequency of pulse generation, tool feed rate, and electrolyte concentration on machining performance, i.e. surface quality, material removal rate (MRR), and accuracy in both macro and micro machining [5, 6]. In addition to process parameters, tool shape and tool paths also affect machining accuracy. Hinduja et al. [7] investigated the final shape of slots machined using a cylindrical and a square tool shape. Their results show that a cylindrical tool produced better machining accuracy than a square tool. They extended their work by using a cylindrical tool to fabricate human-shaped protrusion pockets using zig-zag and contour-parallel tool paths; however, use of a cylindrical tool resulted in tapering of the side walls of the machined feature. Kim et al. [8] reported that micro-scale features machined by a disc-shaped tool had a smaller wall taper than those machined by a cylindrical tool. Recently Goshal et al. [9] proposed a taper reduction technique using a reversed taper tool in micro EC milling. The mentioned works usually used an external nozzle to supply the electrolyte to remove chemical reaction sludge from the gap between workpiece and tool. The effect of the electrolyte flow direction on the side wall of micro grooves has been studied by Chen et al. [10]. Their experimental results showed that using a single nozzle caused the side wall taper to become larger; to reduce the taper, they proposed using a double nozzle flow. The complexity of using an external nozzle can be overcome by ejecting the electrolyte from the tool. Vanderauwera et al. [11] used a hollow copper electrode to produce slots, investigating how the slots final shape was affected by utilizing different cross sections of hollow cylindrical electrodes and various milling parameters such as depth of cut and step-over.

To model the EC milling process, methods are required that can calculate the distribution of current in a three-dimensional domain. Several such methods have been developed; for example, Kozak et al. [12] developed a mathematical model to simulate the workpiece machined by a spherical tool. The current density is assumed to be a linear variation of the electric potential variation between the tool center and the corresponding point on the workpiece surface. Ruszaj et al. [13] presented a mathematical model to calculate the inter-electrode gap size when a rectangular flat-ended tool is moved parallel to the workpiece. The model considers only current flowing in the region directly below the tool end face; stray currents are not considered. Kozak et al. [14] presented a mathematical model to simulate the ECM of complex 3D microstructures produced using pulsed voltage. Liu et al. [15] developed a model to calculate the over-cut of slots machined by a cylindrical electrode with pulsed voltage.

Using numerical techniques such as finite difference method (FDM) or finite element method (FEM) can accurately compute current density on the workpiece surface. However, they are not preferred for use in modeling EC milling because of the difficulty of dynamic 3D-meshing in the entire interior domain bounded by tool and workpiece. This difficulty can be overcome using the boundary element method (BEM), in which only the surfaces of the tool, workpiece, and bounding surfaces have to be discretized. Purcact et al. [16] have presented BEM software to simulate the ECM process in 3D. Pattavanitch et al. [17] used BEM to solve for current density expressed by Laplace's equation in order to model 3D electrochemical milling and turning. More recently Hinduja et al. [7] applied BEM for 3D simulation of a complex pocket shape machined by EC milling.

Tool geometry is also a crucial factor that affects the final shape of EC milled features. Most published research in EC milling has used solid electrodes. There is a very limited amount of work carried out using hollow tools. Thus the purpose of this paper is to numerically and experimentally investigate the final shape of slots on a macro scale using a hollow tool.

2. EXPERIMENTAL SETUP

A schematic diagram of the EC milling setup used in this study is illustrated in Fig. 1. The experiments were performed on a three-axis computer numerical control (CNC) machine which was modified for ECM. The workpiece, which was a rectangular bar made of SS-316, was immersed in an electrolyte in a plastic bath mounted on XY table. The tools were made from high chromium silver steel, with an inner (bore) diameter of 6 mm and an outer diameter of 19 mm. Two tools with different disc diameters were used in the investigation; one had a disc diameter of 12 mm (Fig. 2a) and the other 14 mm (Fig. 2b). In the experiments, a tool was held in a tool holder attached with the Z-axis of the CNC machine.

Sodium Nitrate (NaNO3) at 10% by weight in water was used as the electrolyte. The electrolyte was pumped at high pressure from the tank into the tool holder and through a hollow electrode to reach the machining area.

The applied voltage was generated by an external DC power supply. The CNC table was driven by stepper motors with a resolution of 0.1 mm, and the movements of the table were computer-controlled.

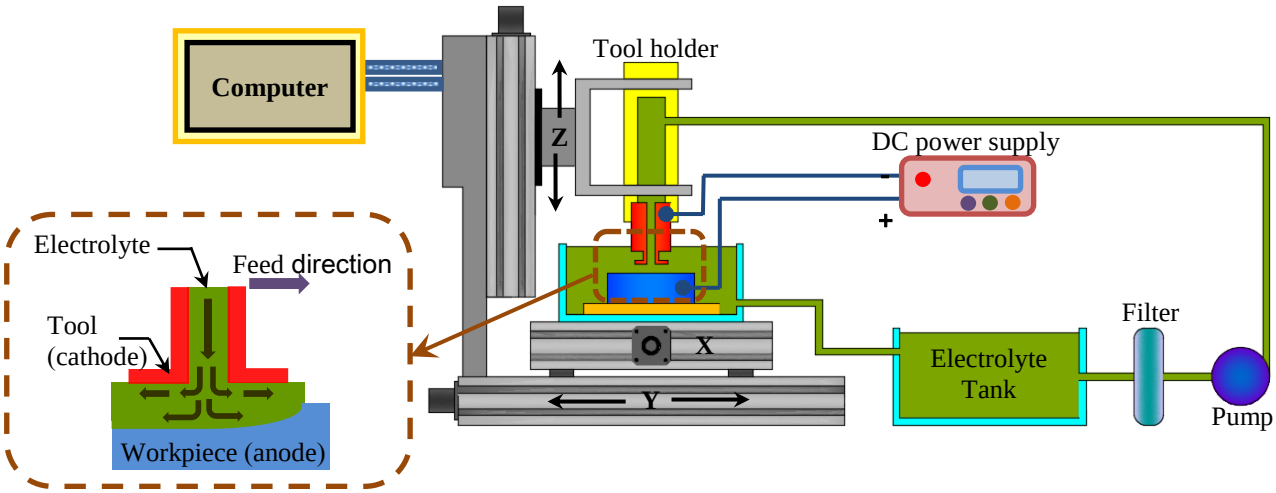

Fig. 1. Schematic diagram of the experimental setup.

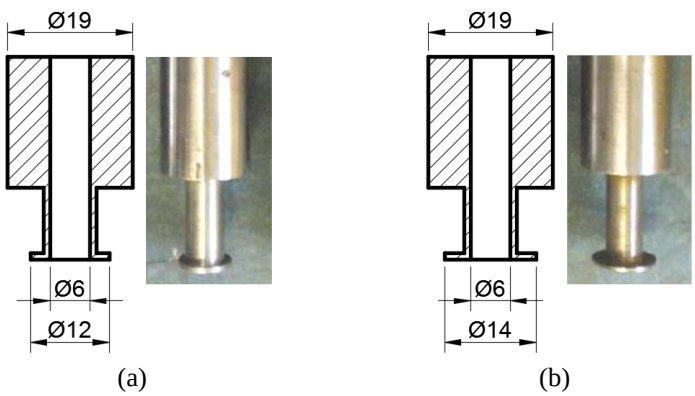

Fig. 2. Milling tool, (a) outer diameter 12 mm, (b) outer diameter 14 mm.

In this work, slots were machined by travelling the tool from one end of the slot (point A in Fig. 3.) to the other end (point B) at a specified feed rate and applied voltage. The total length of the tool path was 50 mm. Three cross section profiles of the slot were measured, one at 7.5 mm from the entrance edge (section A-A in Fig. 4.), another one at the middle section of the slot (section B-B) and the last one at 22.5 mm from the entrance edge (section C-C). The profiles were measured using a laser profiler machine.

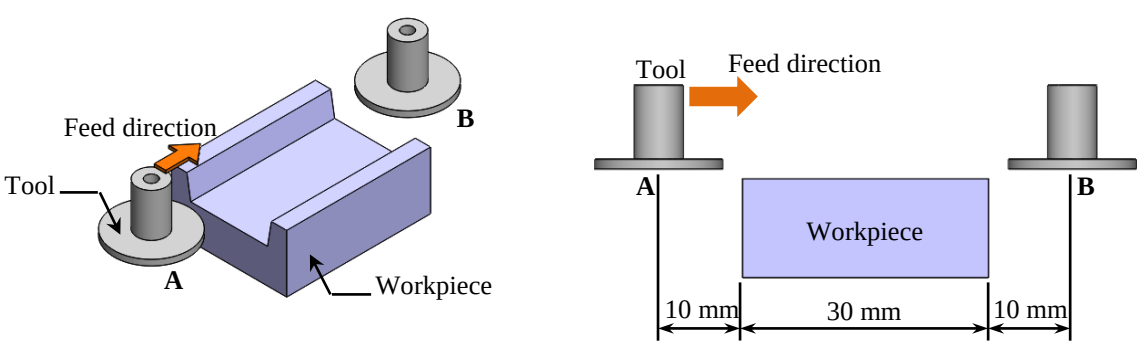

Fig. 3. The tool path for slot machining.

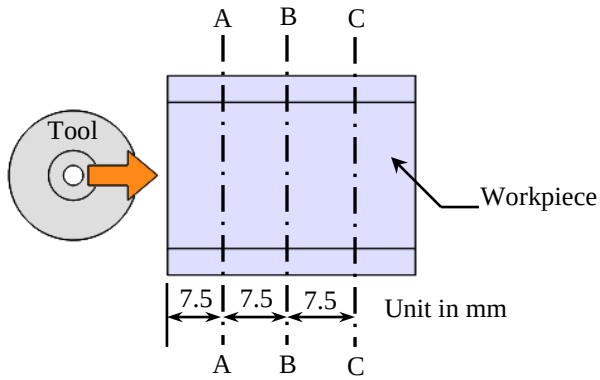

Fig. 4. Position of cross section profiles.

3. BOUNDARY ELEMENT MODEL

Referring to the experimental setup (Fig. 1.), a 3D model can be created with BEM by forming a closed shell of interconnected faces, some faces of which belong to the tool, represented by a hollow cylinder (red faces), and others to the workpiece (dark blue faces). The remaining faces (light blue) are the boundary faces which are sufficiently far away from the tool and workpiece surfaces so as not to influence the computed results, as illustrated in Fig. 5.

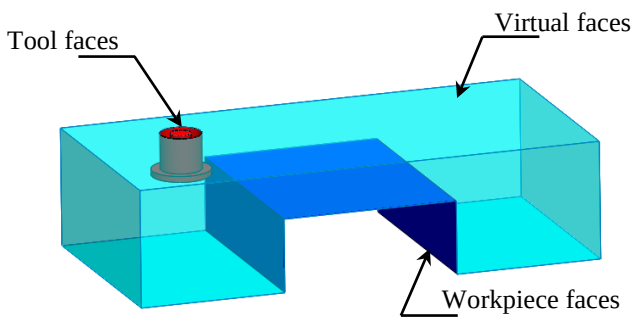

Fig. 5. BEM domain for EC milling.

Once the domain is created with the BEM, only the bounding faces of the domain have to be discretized as 2D elements. Hence, linear triangular elements were used to discretize the domain since they are able to approximate both regular and free-form surfaces. The base face of the tool and the top surface of the workpiece were discretized with fine structured meshes (Fig. 6a) because these faces affect the accuracy of the computed results. Since the virtual surfaces have no effect on the predicted shape of the workpiece, they were discretized with coarse unstructured meshes. The complete mesh is shown in Fig. 6b.

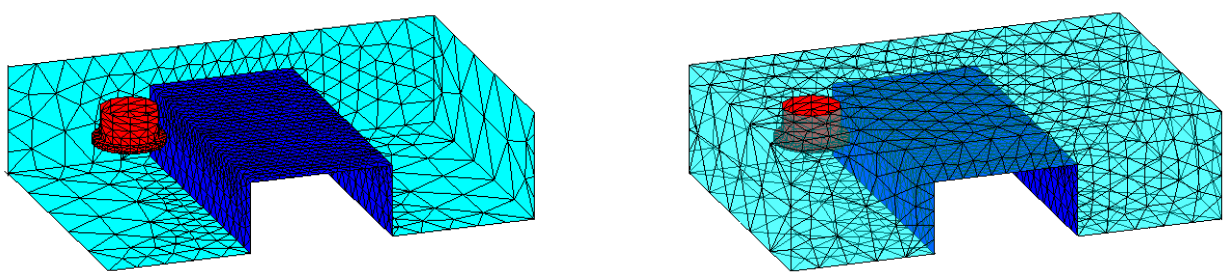

Fig. 6. (a) Meshes created on the surface of the domain and (b) the complete discretized 3D domain.

In ECM, the density distribution of current in the gap between the tool and workpiece surfaces is governed by Laplace's equation:

$$\nabla^2 U = 0 \tag{1}$$

In general, BEM equations can be expressed in matrix form as:

$$[H][U] = [G][q] \tag{2}$$

The matrices $[U]$ and $[q]$ are matrices for the value of voltage (U) and voltage gradient (dU/dn) of each node on the domain surfaces. $[H]$ and $[G]$ are matrices depending on the geometry and boundary conditions of the domain.

Since the tool was not insulted, all faces of the tool were assumed to be at 0 volt. The workpiece surfaces have the condition $U = V - \eta$ imposed on them, V and η being the applied voltage and total over-potential, respectively. Since the virtual surfaces are far away from the tool surface, they were assumed to be completely insulated $(dU/dn = 0)$.

The solution of equation (2) yields the voltage and voltage gradient at any point in the domain. Then, the current density (J) can be calculated using the known electrolyte conductivity (κ_e) as:

$$J = \kappa_e \frac{dU}{dn} \tag{3}$$

The assumptions made in the analysis are that electrical conductivity of the electrolyte is constant across the entire gap; the effects of heat, bubbles, or metal film generated during machining are not considered; and at each time step of the analysis, the phenomena occurring in the domain are assumed to be in steady state condition.

In the analysis, the total machining time has to be divided into small time steps (Δt). During each time step, the tool is moved in the feed direction by a distance of Δs $(\Delta s = \textit{feed rate} \times \Delta t)$. The current density and amount of machining taking place at each node on the workpiece surface are calculated. Based on Faraday's law, the workpiece shape after each time step was determined by moving each node by a distance Δh in a direction normal to the surface of the node [18].

$$\Delta h = \varepsilon \frac{M \times J \times \Delta t}{\rho \times z \times F} \tag{4}$$

where M is the atomic weight of workpiece material, F the Faraday's constant, z the valence electron, ε the current efficiency and ρ the workpiece material density.

Since the nodes on workpiece surfaces are move at the end of every time step, some elements become distorted and the quality becomes poor. To deal with this problem, the distorted or stretched elements on the workpiece have to be modified using subdivision mesh refinement techniques [19]. Also at the end of every time step, the tool surfaces have to be translated, causing compression of some elements. This problem was solved by deleting and re-generating the mesh on the top virtual face.

4. NUMERICAL AND EXPERIMENTAL RESULTS AND DISCUSSION

In the experiments, a slot was machined in a single pass at two different applied voltages, 12V and 18V, and two different feed rates, 2 mm/min and 6 mm/min. The initial gap of machining was 0.2 mm.

According to the concentration of electrolyte in the experiment, from preliminary tests, the process parameters for BEM were: $\eta = 1.5V$, $\varepsilon = 85\%$, and $\kappa_e = 0.025 S/mm$. To prevent oscillation in computation, the time step (Δt) required to be used for BEM is 0.1s [17].

From the preliminary investigation of optimal size of the element on workpiece of BE model, it was found that the optimal element size (i.e. the diameter of the circumcircle which passes through all three vertices of a triangular element) is 0.06 mm. Decreasing the element size beyond the optimal size, yields similar results but the computing time is increased considerably. Hence, the BE model initially consisted of 63,245 elements.

The actual slots machined by the hollow tool with 12 mm and 14 mm outer diameter are shown in Fig. 7 (a) and (b), respectively. Fig. 8 shows a 3D view of the slot predicted by the BE model.

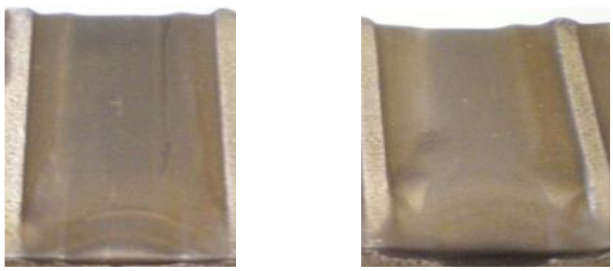

(a) (b)

Fig. 7. Actual slots machined by the hollow tool with outer diameter (a) 12 mm and (b) 14 mm.

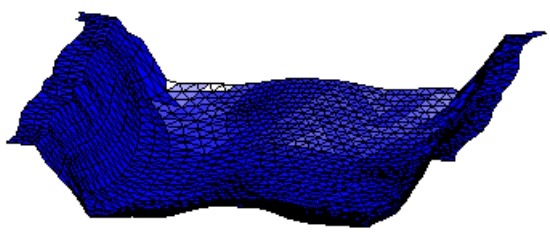

Fig. 8. 3D view of a slot predicted by BE model.

The cross-section profiles at the middle of the slots machined in the experiments using tools with an outer diameter of 12 mm and of 14 mm are shown in Fig. 9 and Fig. 10, respectively; the profiles obtained from BE model are also included for comparison purposes.

These profiles from experiments and BE model are similar in the sense that the side walls of the slots are not vertical, the junction between the side walls and the base surface is rounded, and the bottom surface is not flat. Instead there is a bulge at the center of the bottom, and the shape of this bulge resembles part of a sinusoidal profile. This bulge has its peak directly below the center of the through hole.

To assess the performance of machining and to evaluate the accuracy of the BE model results, the values of slot parameters, namely width (W), depth (D), and the distance to the highest point of the bulge (DB), are measured (see Fig. 11.) at each section. The average values of slot parameters at each section as obtained from actual machining and BE model are given in Table 1.

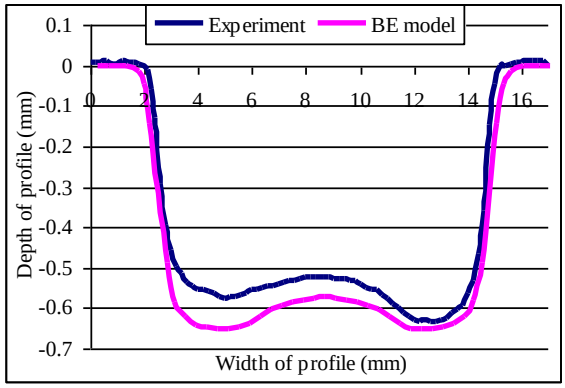

(Test 1)

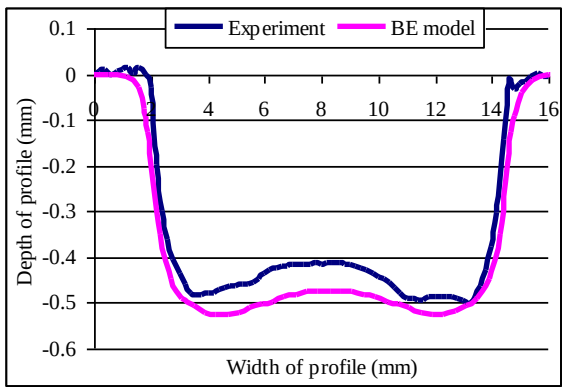

(Test 2)

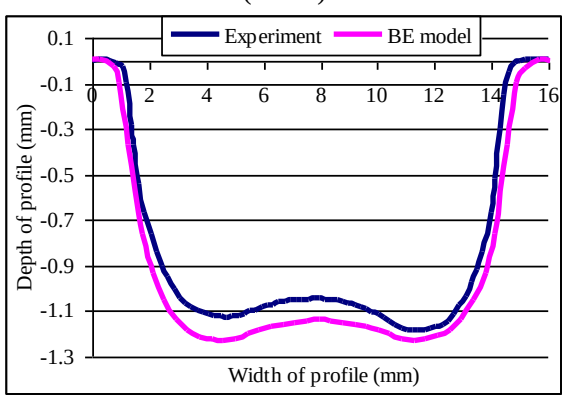

(Test 3)

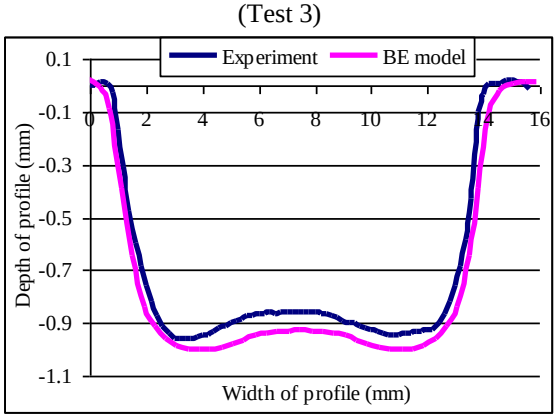

(Test 4)

Fig. 9. Cross-section of slot machined with tool outer diameter 12 mm.

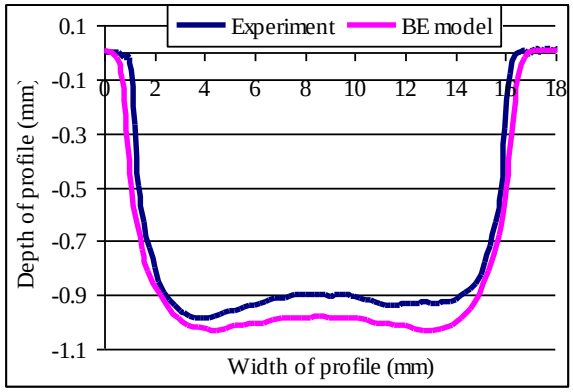

(Test 5)

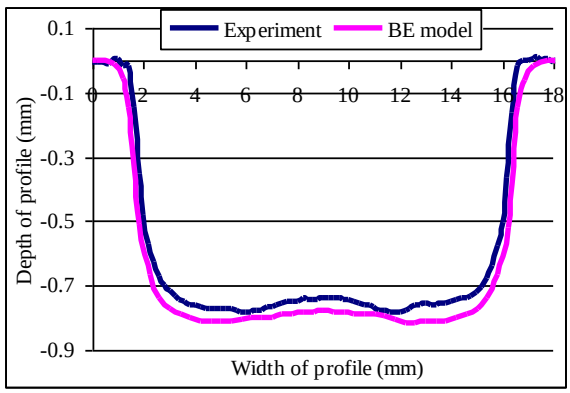

(Test 6)

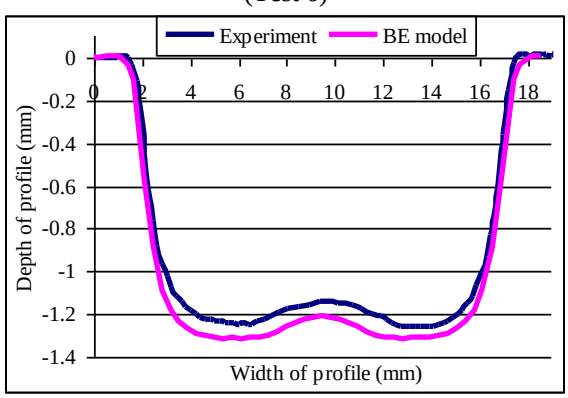

(Test 7)

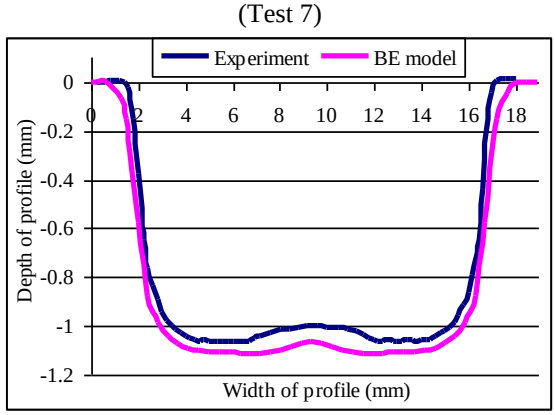

(Test 8)

Fig. 10. Cross-section of slot machined with tool outer diameter 14 mm.

.

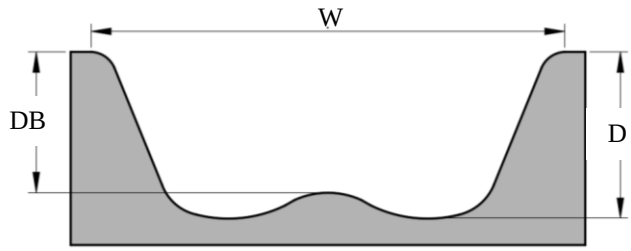

Fig. 11. The measurement of values of slot parameters.

Table1: Average value of slot parameters obtained experimentally and numerically.

		Test number							
		1	**2**	**3**	**4**	**5**	**6**	**7**	**8**
Tool diameter (mm)		12	12	12	12	14	14	14	14
Voltage (V)		12	12	18	18	12	12	18	18
Feed Rate (mm/min)		2	6	2	6	2	6	2	6
Width (mm)	**Experiment**	13.01	12.83	13.80	13.21	15.41	15.20	16.40	15.80
	BE model	13.78	13.88	14.90	14.32	16.23	16.41	17.21	16.95
	Error (%)	5.91	8.18	7.97	8.40	5.39	7.89	4.93	7.28
Depth (mm)	**Experiment**	0.61	0.49	1.18	0.96	0.98	0.78	1.26	1.08
	BE model	0.65	0.53	1.23	1.01	1.03	0.81	1.31	1.12
	Error (%)	6.55	8.16	4.23	5.21	5.10	3.84	3.96	3.70
Distance to Bulge (mm)	**Experiment**	0.52	0.42	1.04	0.86	0.88	0.74	1.14	0.99
	BE model	0.57	0.47	1.13	0.93	0.98	0.78	1.21	1.07
	Error (%)	9.61	11.90	8.65	8.14	11.36	5.41	6.14	8.08

The results show that for a specific applied voltage, the overcut (i.e. the error of machining: the difference between slot width and the tool diameter) and the slot depth increase as the tool feed rate decreases. For example, at an applied voltage of 12V, the overcut and depth of the slot machined at a 6 mm/min tool feed rate (Test 2) are 0.83 (12.83-12) mm and 0.49 mm , respectively, and they increase to 1.01 (13.01-12) mm and 0.61 mm, respectively, when the feed rate is reduced to 2 mm/min (Test 1).

On the other hand, at a specific feed rate, both the overcut and depth of slot increase with increasing applied voltage. For example, at 6 mm/min tool feed rate, when the applied voltage changes from 12V (Test 2) to 18V (Test 4), the overcut increases from 0.83 (12.83-12) mm to 1.21 (13.21-12) mm, and the slot depth increases from 0.49 mm to 0.96 mm.

This is reasonable because when the tool feed rate decreases, a unit area of the workpiece sees the tool for a longer time, and as a result more material is removed. Similarly when the applied voltage increases, there will be a corresponding increase in the current density value, causing a greater amount of material to be removed.

The results also show that under the same machining conditions, when the tool diameter increases, the overcut and depth of the slot increase. For example, the overcut and depth of a slot machined by a tool of diameter 12 mm (Test 3) are 1.80 (13.80-12) mm and 1.18 mm, respectively, and they increase to 2.40 (16.40-14) mm and 1.26 mm when the tool with diameter of 14 mm is used to produce the slot (Test 7).

The reason for this is that when the surface area of the tool increases, the localization effect of current flux flow increases, which in turn causes the stray current to increase, resulting in more material being removed, i.e. greater overcut and depth.

Since the tool had a central through hole for the electrolyte to flow, the current density distribution on the workpiece surface in the region directly under the tool is non-uniform (see Fig. 12(a)). BE model analysis (see Fig. 12(b)) showed that the current density on the workpiece surface directly below the end of the tool surface was

higher (the orange-red region) than that on the workpiece surface directly below the central hole (the cyan-blue region). This results in a greater MRR at the workpiece surface below the end of the tool than that at the surface below the central hole. Consequently, the bulge occurs at the center of the slot.

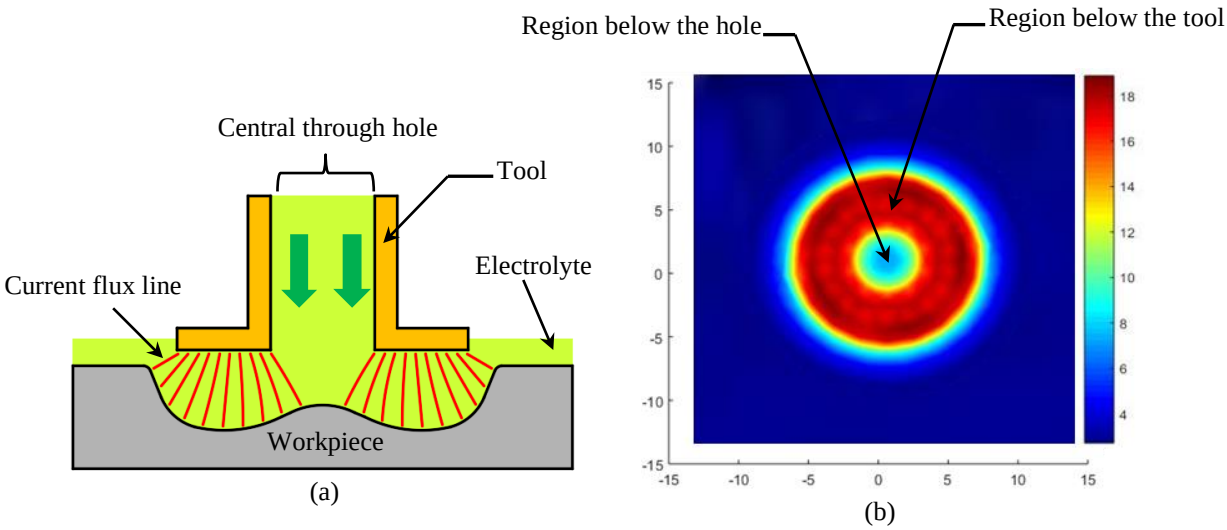

Fig. 12. (a) Schematic view of current flux line from the tool to the workpiece and (b) distribution of the current density on the workpiece surface.

The experimental results reveal that the height of the bulge (i.e. the difference between the highest and the lowest points on the slot surface: D – DB) depends on the applied voltage and the tool feed rate. In other words, for the same tool diameter, the higher the applied voltage and lower the feed rate, the greater the height of the bulge. For example, in the profiles of slots machined by a tool with an outer diameter of 12 mm, when the applied voltage is increased from 12V (Test 1) to 18V (Test 3), the bulge height increases from 0.09 (0.61 - 0.52) mm to 0.14 (1.18 - 1.04) mm. Similarly, when the feed rate is decreased from 6 mm/min (Test 4) to 2 mm/min (Test 3), the height of the bulge increases from 0.1 (0.96 - 0.86) mm to 0.14 mm (1.18 - 1.04).

Comparisons between the profiles obtained experimentally and from BE model show agreement; however, in all cases the BE model profiles are deeper and have a greater overcut than those obtained experimentally. From Table 1, the average difference between the experimental and BE model values is 6.92%, with the maximum error being 11.9%. This is because in simulation, the values of over-potential, electrolyte conductivity, and current efficiency are assumed to be constant during machining. However, in actual practice, these values vary with electrolyte temperature and flow conditions, i.e. laminar or turbulent conditions. Hence, flux density calculated by BE model is overestimated, with BE model predicting a greater amount of material machined than what occurs in actual machining.

5. CONCLUSION

Slot features were experimentally and numerically investigated by electrochemical milling using hollow tool geometry. The central hole of the tool caused a bulge to present on the bottom face of the slot, with its peak directly below the center of the through hole. The overcut, depth, and bulge distance of a slot depend not only on machining parameters such as tool feed rate and applied voltage, but also on the tool diameter. Under the same machining conditions, the parameters of a slot machined by a bigger diameter tool have greater values than those of slots machined by a smaller diameter tool. The cross-section profile shapes predicted by BE model were in agreement with the actual slots machined in the experiment; the average error in predicted versus experimentally machined values of the slot parameters was 6.92%.

ACKNOWLEDGEMENT

This research was made possible through financial support from the National Science and Technology Development Agency, Thailand (NSTDA) under grant number SCH-NR2016-251.

REFERENCES

[1] Li, Z. and Ji, H. Machining accuracy prediction of aero-engine blade in electrochemical machining based on BP neural network, paper presented in the 2009 International Workshop on Information Security and Application, 2009, Qingdao, China.
[2] Walker, J.C., Kamps, T.J., Lam, J.W., Mitchell-Smith, J. and Clare, A.T. Tribological behaviour of an electrochemical jet machined textured Al-Si automotive cylinder liner material, Wear, Vol. 376-377(Part B), 2017, pp. 1611-1621.
[3] Kamaraj, A.B., Sundaram, M.M. and Mathew, R. Ultra high aspect ratio penetrating metal microelectrodes for biomedical applications, Microsyst Technol., Vol. 19, 2013, pp. 179-186.
[4] Singh, J., Jain, V.K. and Ramkumar, J. Fabrication of complex circuit on printed circuit board (PCB) using electrochemical micro-machining, Int. J. Adv. Manuf. Technol., Vol. 85, 2016, pp. 2073-2081.
[5] Mishra, K., Dey, D., Sarkar, B.R. and Bhattacharyya, B. Experimental investigation into electrochemical milling of Ti6Al4VK, J. Manuf. Processes, Vol. 29, 2017, pp. 113-123.
[6] Ghoshal, B. and Bhattacharyya, B. Generation of microfeatures on stainless steel by electrochemical micromachining, Int. J. Adv. Manuf. Technol., Vol. 76, 2015, pp. 39-50.
[7] Hinduja, S. and Pattavanitch, J. Experimental and numerical investigations in electro-chemical milling, CIRP Journal of Manufacturing Science and Technology, Vol. 12, 2016, pp. 79-89.
[8] Kim, B.H., Ryu, S.H., Choi, D.K. and Chu, C.N. Micro electrochemical milling, J. Micromech. Microeng., Vol. 15, 2005, pp. 124-129.
[9] Ghoshal, B. and Bhattacharyya, B. Investigation on profile of microchannel generated by electrochemical micromachining, J. Mater. Process. Technol., Vol. 222, 2015, pp. 410-421.
[10] Chen, C., Li, J., Zhan, S., Yu, Z. and Xu, W. Study of micro groove machining by micro ECM, Procedia CIRP., Vol. 42, 2016, pp. 418-422.
[11] Vanderauwera, W., Vanloffelt, M., Perez, R. and Lauwersa, B. Investigation on the performance of macro electrochemical milling, Procedia CIRP., Vol. 6, 2013, pp. 356-361.
[12] Kozak, J., Chuchro, M., Ruszaj, A. and Karbowski, K. The computer aided simulation of electrochemical process with universal spherical electrodes when machining sculptured surfaces, J. Mater. Process. Technol., Vol. 107, 2000, pp. 283-287.
[13] Ruszaj, A. and Zybura-Skrabalak, M. The mathematical modelling of electrochemical machining with flat ended universal electrodes, J. Mater. Process. Technol., Vol. 109, 2001, pp. 333-338.
[14] Kozak, J., Rajurkar, K.P. and Makkar, Y. Study of pulse electrochemical micromachining, J. Manuf. Processes, Vol. 6, 2004, pp.7-14.
[15] Liu, Y., Zhu, D. and Zhu, L. Micro electrochemical milling of complex structures by using in situ fabricated cylindrical electrode, Int. J. Adv. Manuf. Technol., Vol. 60, 2012, pp. 977-984.
[16] Purcar, M., Bortels, L., Van den Bossche, B. and Deconinck, J. 3D Electrochemical machining computer simulations, J. Manuf. Processes, Vol. 149, 2004, pp.472-478.
[17] Pattavanitch, J., Hinduja, S. and Atkinson, J. Modelling of the electrochemical machining process by the boundary element method, CIRP Annals, Vol. 59(1), 2010, pp. 243-246.
[18] McGeough, J.A. Principles of Electrochemical Machining, 1975, Chapman and Hall, UK.
[19] Miguel, A.P., Jose, P.S., and Angel, P. Refinement based on longest-edge and self-similar four-triangle partitions, Mathematics and Computers in Simulation, Vol. 75, 2006, pp.251-262.